ACS APPLIED MATERIALS & INTERFACES

Research Article

www.acsami.org

Temperature-Dependent Raman Spectroscopy of Titanium Trisulfide (TiS_3) Nanoribbons and Nanosheets

Amit S. Pawbake,[†,⊥] Joshua O. Island,[‡] Eduardo Flores,[§] Jose Ramon Ares,[§] Carlos Sanchez,[§] Isabel J. Ferrer,[§] Sandesh R. Jadkar,[†] Herre S. J. van der Zant,[‡] Andres Castellanos-Gomez,*[,∥] and Dattatray J. Late*[,⊥]

[†]School of Energy Studies, Department of Physics, Savitribai Phule Pune University, Pune 411007, India

[‡]Kavli Institute of Nanoscience, Delft University of Technology, Lorentzweg 1, 2628 CJ Delft, The Netherlands

[§]Materials of Interest in Renewable Energies Group (MIRE Group), Departamento de Física de Materiales, Universidad Autónoma de Madrid, UAM, 28049 Madrid, Spain

[∥]Instituto Madrileño de Estudios Avanzados en Nanociencia (IMDEA Nanociencia), Campus de Cantoblanco, E-28049 Madrid, Spain

[⊥]Physical & Materials Chemistry Division, CSIR-National Chemical Laboratory, Dr. Homi Bhabha Road, Pune 411008, India

ABSTRACT: Titanium trisulfide (TiS_3) has recently attracted the interest of the 2D community because it presents a direct bandgap of ~1.0 eV, shows remarkable photoresponse, and has a predicted carrier mobility up to 10000 $cm^2 V^{-1} s^{-1}$. However, a study of the vibrational properties of TiS_3, relevant to understanding the electron−phonon interaction that can be the main mechanism limiting the charge carrier mobility, is still lacking. In this work, we take the first steps to study the vibrational properties of TiS_3 through temperature-dependent Raman spectroscopy measurements of TiS_3 nanoribbons and nanosheets. Our investigation shows that all the Raman modes linearly soften (red shift) as the temperature increases from 88 to 570 K due to anharmonic vibrations of the lattice, which also includes contributions from the lattice thermal expansion. This softening with the temperature of the TiS_3 modes is more pronounced than that observed in other 2D semiconductors, such as MoS_2, $MoSe_2$, WSe_2, and black phosphorus (BP). This marked temperature dependence of the Raman spectra could be exploited to determine the temperature of TiS_3 nanodevices by using Raman spectroscopy as a noninvasive and local thermal probe. Interestingly, the TiS_3 nanosheets show a stronger temperature dependence of the Raman modes than the nanoribbons, which we attribute to lower interlayer coupling in the nanosheets.

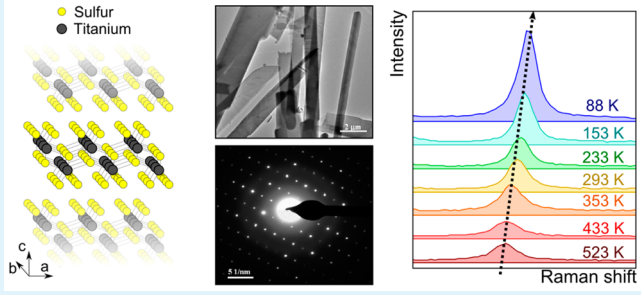

KEYWORDS: *TiS_3 nanoribbons, TiS_3 nanosheets, Raman spectroscopy, thermal effect, layered materials, 2D semiconductors*

1. INTRODUCTION

Upon the isolation of graphene,[1] a large number of 2D inorganic layered materials have been investigated[2,3] The transition metal dichalcogenide (TMDC) family is among those that have raised the largest amount of interest in the nanoscience and material science communities as its members present a large variety of electronic properties (ranging from wide band gap semiconductors to superconductors that possess Peierls instability and display charge density wave transport).[4−9] The semiconducting TMDCs (MoS_2, $MoSe_2$, WS_2, and WSe_2) are especially relevant because of their potential in various types of nanodevices, including photodetectors,[10−13] field effect transistors,[14−19] gas sensors,[20] solar cells,[21−25] energy storage devices,[26] and field emitters.[27]

Besides the TMDC family, the trichalcogenide family (with general formula MX_3; M = Ti, Zr, Hf, Nb, Ta; X = S, Se, Te) promises the same richness of electronic and optical properties but remains almost unexplored.[28−30] Within the trichalcogenide family members, titanium trisulfide (TiS_3) has recently attracted the interest of the 2D community as it has been demonstrated that single layers of TiS_3 can be isolated by mechanical exfoliation, and field-effect transistors and photodetectors can be realized.[31,32] Unlike Mo- and W-based dichalcogenides (which present a direct bandgap only at the single-layer limit), TiS_3 has a direct bandgap of ~1.0 eV, which is optimal for photovoltaic and photocatalysis applications.[33−35] Moreover, recent theoretical works predict that the ideal carrier mobility of TiS_3 can reach values as high as 10000 $cm^2 V^{-1} s^{-1}$.[36] A study of the vibrational properties of trichalcogenides is important to understand their electron−phonon interaction, which plays an important role in the electronic performance of nanodevices and can even be the main mechanism limiting the

Received: August 13, 2015
Accepted: October 15, 2015
Published: October 15, 2015

DOI: 10.1021/acsami.5b07492
ACS Appl. Mater. Interfaces 2015, 7, 24185−24190

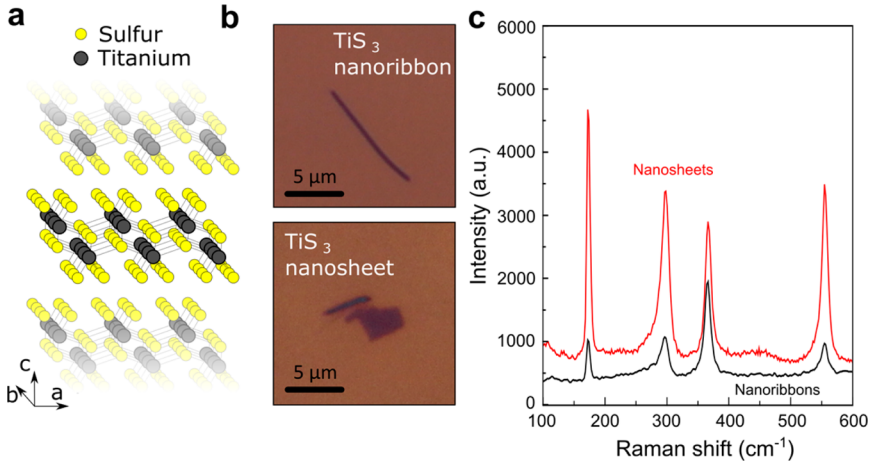

Figure 1. (a) Schematic diagram of the TiS_3 crystal structure. (b) Optical microscopy images of a TiS_3 nanoribbon (grown at 550 °C) and a TiS_3 nanosheet (grown at grown at 400 °C) deposited onto a SiO_2/Si substrate. (c) Raman spectra of TiS_3 nanoribbon and nanosheet samples recorded at room temperature using a 532 nm Ar laser source with 5 mW power.

charge carrier mobility.[37] However, a systematic study of the vibrational properties of TiS_3 at different temperatures is still lacking.

In this work, we study the vibrational properties of TiS_3 by means of Raman spectroscopy performed over a wide range of temperatures from 88 to 570 K. Two sets of TiS_3 samples, synthesized at different temperatures, were studied: TiS_3 nanoribbons (grown at 550 °C) and TiS_3 nanosheets (grown at 400 °C).[32] The samples were characterized by X-ray diffraction, transmission electron microscopy and electron diffraction, showing that both sets of samples present high crystallinity. Their Raman spectra showed four prominent peaks corresponding to the excitation of A_g-type Raman modes, whose frequencies exhibit a linear temperature dependence over the entire temperature range from 88 to 570 K. The first order temperature coefficients (χ) associated with each Raman mode have been extracted from the measured temperature dependence. This variation with temperature, similar to that observed in other 2D systems, is mainly attributed to the anharmonic vibrations of the lattice, which includes contributions from the lattice thermal expansion due to anharmonicity. Interestingly, the temperature dependence of the Raman spectrum of TiS_3 nanosheets is noticeably stronger than that of TiS_3 nanoribbons, which might indicate a lower interlayer coupling for nanosheets than for nanoribbons.

2. RESULTS AND DISCUSSION

Figure 1(a) shows the TiS_3 monolayer structure where the dark gray and yellow spheres refer to Ti and S, respectively. As pointed out in the Introduction, two sets of TiS_3 samples were studied in this work: TiS_3 nanoribbons (grown at 550 °C) and TiS_3 nanosheets (grown at 400 °C). We address the reader to ref 32 and to the Materials and Methods for more details on the TiS_3 synthesis. Figure 1(b) shows an example of a TiS_3 nanoribbon (~30-nm thick) and a TiS_3 nanosheet (~5-nm thick) deposited onto a SiO_2/Si substrate by means of an all-dry transfer technique. Independent of their morphology, TiS_3 nanoribbons and nanosheets present similar Raman spectra (see Figure 1(c)) and have the same stoichiometry and crystal structure. For the temperature-dependent Raman spectrum measurements, the as-prepared TiS_3 nanoribbon and nanosheet powders (mainly containing ribbons and flakes 100−300-nm thick)[32] were simply deposited onto SiO_2/Si substrates.

Concerning the space group of MX_3 trichalcogenides (M = Ti, Zr, Hf) and (X = S, Se), there are two stable structures: A ($ZrSe_3$-type) and B (TiS_3-type). Both structures belong to the $P2_1/m$ space group (monoclinic).[38] The TiS_3 samples have been structurally characterized using X-ray diffraction (XRD) in a Panalytical X'pert Pro X-ray diffractometer (Cu Kα radiation (λ = 1.5406 Å), and all the studied TiS_3 samples belongs to the B variant. Typical XRD patterns of TiS_3 nanoribbon samples are shown in Figure 2. A preferential growth in the (001) direction can be easily seen, which is common of the MX_3 family. Its composition, analyzed by energy dispersive X-ray (EDX Analyzer INCA x-sight) at 20 keV electron beam energy results in a stoichiometric ratio of S/Ti = 2.9 ± 0.2. We address the reader to ref 32 to find the XRD and EDX characterizations of the TiS_3 nanosheet samples.

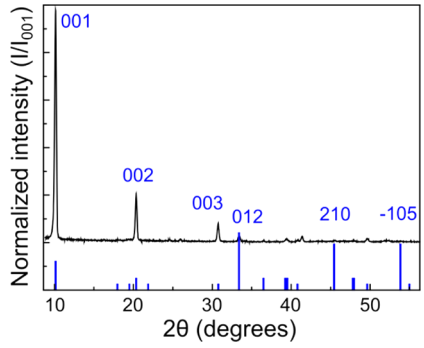

Figure 2. XRD diffraction pattern of TiS_3 nanoribbons synthesized at 550 °C. Lines corresponding to the monoclinic phase TiS_3 (P12/m) as tabulated in JCPDS 015-0783 are included.

Panels a and b in Figure 3 show transmission electron microscopy (TEM) images of several TiS_3 nanoribbons. Figure 3(c) shows a high resolution (HR) TEM image of a TiS_3 nanoribbon showing lines spaced by ~0.41 nm, which matches with the distance along the "*a*" direction of the lattice (JCPDS-ICDD 15-0783) if the sample is observed at an angle of 30° from the (011) crystal plane. Figure 3(d) shows the selected area electron diffraction (SAED) pattern of the TiS_3 nano-

DOI: 10.1021/acsami.5b07492
ACS Appl. Mater. Interfaces 2015, 7, 24185−24190

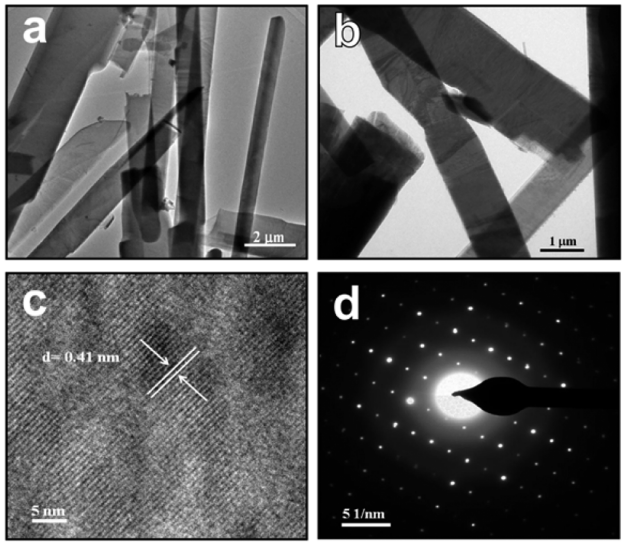

Figure 3. (a and b) Low resolution TEM images of several TiS_3 nanoribbons. (c) HRTEM image of a TiS_3 nanoribbon. (d) Selected area electron diffraction (SAED) pattern for the TiS_3 nanoribbon.

ribbon indicating the high crystalline nature of the sample. Panels a and b in Figure 4 show typical low magnification TEM

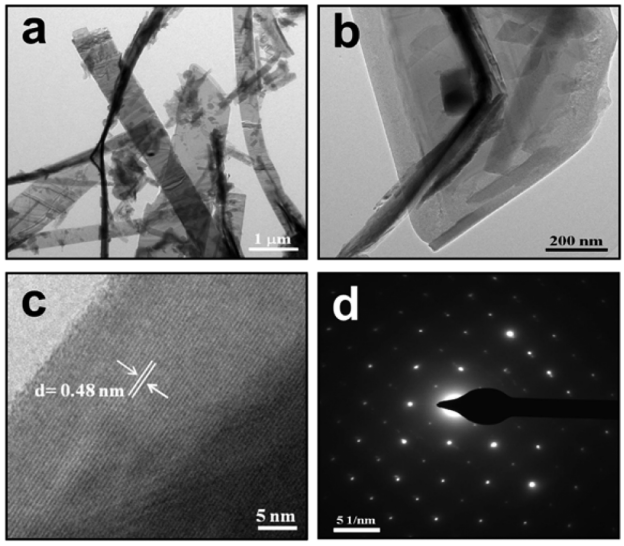

Figure 4. (a and b) Low resolution TEM images of several TiS_3 nanosheets. (c) HRTEM image of a TiS_3 nanosheet. (d) Selected area electron diffraction (SAED) pattern for the TiS_3 nanosheet.

images of several TiS_3 nanosheets. Figure 4(c) shows an HRTEM image of a TiS_3 nanosheet showing lines spaced by ~0.48 nm, which matches very well with the distance along the "*a*" direction of the lattice (JCPDS-ICDD 15-0783) if the sample is observed almost perfectly aligned with the (011) crystal plane. Figure 4(d) shows the SAED pattern of the TiS_3 nanosheet indicating the high crystalline nature of the TiS_3 nanosheet sample.

The Raman spectrum of TiS_3 nanoribbons and nanosheets shows four prominent A^1_g modes that appear at ~172, 296, 366, and 554 cm^{-1} (labeled hereafter as *I*, *II*, *III* and *IV*) due to the in-plane and out-of-plane vibration modes (see Figure 1(b)).[39] Figure 5 shows the temperature-dependent Raman spectra of a few-layer TiS_3 nanoribbon and nanosheet sample recorded at various temperatures from 88 to 570 K. It is observed that, for both samples, the Raman spectra peak positions of all modes shift toward lower wavenumbers when the temperature is increased from 88 to 570 K. Similar behavior has been observed for other 2D materials (such as graphene, graphene oxide, MoS_2, $MoSe_2$, WSe_2, and BP) and it has been attributed to the anharmonic coupling of phonons and the thermal expansion of the lattice that changes the equilibrium positions of the atoms, changing the interatomic forces, and thus the phonon energies.[40−44] We also observed that the full-width at half-maximum (fwhm) for all Raman modes increased with an increase in temperature. The evolution of the Raman peak position, ω, follows a linear dependence with the temperature

$$\omega(T) = \omega_0 + \chi T \quad (1)$$

where ω_0 is the peak position of the vibration mode at zero Kelvin temperature, and χ is the first-order temperature coefficient of the respective Raman mode. Here, nonlinear coefficients have not been considered as they are only relevant at higher temperatures.

Figure 6 shows the temperature evolution of the four Raman modes measured for the nanoribbon (empty symbols) and nanosheet (filled symbols) samples. The first-order temperature coefficients for the different Raman modes χ_i can be determined from a linear fit. For the TiS_3 nanoribbons, the first-order temperature coefficients are $\chi_I = -0.008$ cm^{-1} K^{-1}, $\chi_{II} = -0.018$ cm^{-1} K^{-1}, $\chi_{III} = -0.021$ cm^{-1} K^{-1}, and $\chi_{IV} = -0.018$ cm^{-1} K^{-1}. For the nanosheets, the first-order temperature coefficients are found to be $\chi_I = -0.022$ cm^{-1} K^{-1}, $\chi_{II} = -0.025$ cm^{-1} K^{-1}, $\chi_{III} = -0.024$ cm^{-1} K^{-1}, and $\chi_{IV} = -0.017$ cm^{-1} K^{-1}. The temperature evolution of the Raman modes of TiS_3 is more pronounced than that reported for other 2D semiconductor materials (MoS_2,[41] $MoSe_2$,[45] WS_2,[43] WSe_2,[45] or black phosphorus,[44] which are summarized in Table 1), and thus, our temperature-dependent Raman study can be exploited as a noninvasive local probe to measure the temperature in TiS_3-based nanodevices.

From Figure 6, it is also clear that the temperature effect on the Raman modes of TiS_3 nanosheets is stronger than that observed in nanoribbons. This effect can be attributed to a reduced interaction between the TiS_3 layers in the nanosheet sample that would lead to an enhanced in-plane thermal expansion. The mode at ~170 cm^{-1} shows the most pronounced difference between nanosheets and nanoribbons, indicating that it is probably an antiphase out-of-plane mode where the vibration of the lattice substantially changes the interlayer distance during the oscillation. However, to our knowledge, the exact shape of the Raman vibrational modes in TiS_3 is still unclear. In fact, the XRD data presented in ref 32 show how the interlayer distance for the TiS_3 nanosheets is 0.2% larger than that measured for TiS_3 nanoribbons. A similar effect of the interlayer interaction on the first-order temperature coefficient has been observed by Calizo et al. in graphene samples.[46] They noted how the temperature coefficient varied inversely with the number of graphene layers, being much larger for single layer graphene (no interlayer interaction) than that for highly oriented pyrolytic graphite.

3. CONCLUSIONS

In summary, we present a study of the vibrational properties of TiS_3 by means of Raman spectroscopy over a wide range of temperatures. We studied TiS_3 samples with two different

DOI: 10.1021/acsami.5b07492
ACS Appl. Mater. Interfaces 2015, 7, 24185−24190

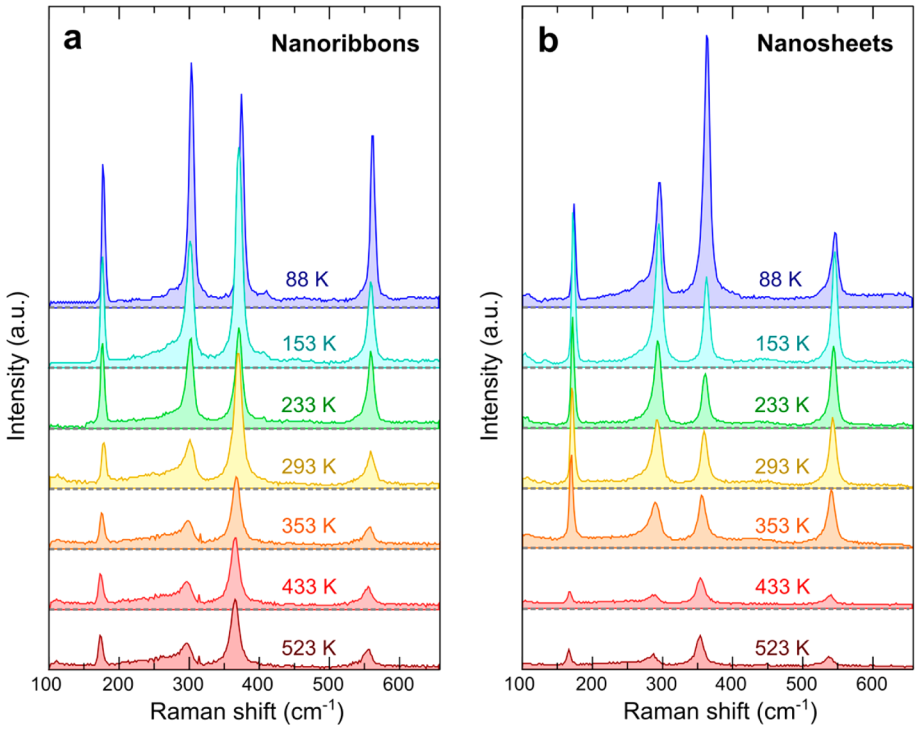

Figure 5. Raman spectra of a (a) TiS_3 nanoribbon and (b) TiS_3 nanosheet sample recorded at various temperatures, acquired with a 532 nm excitation laser.

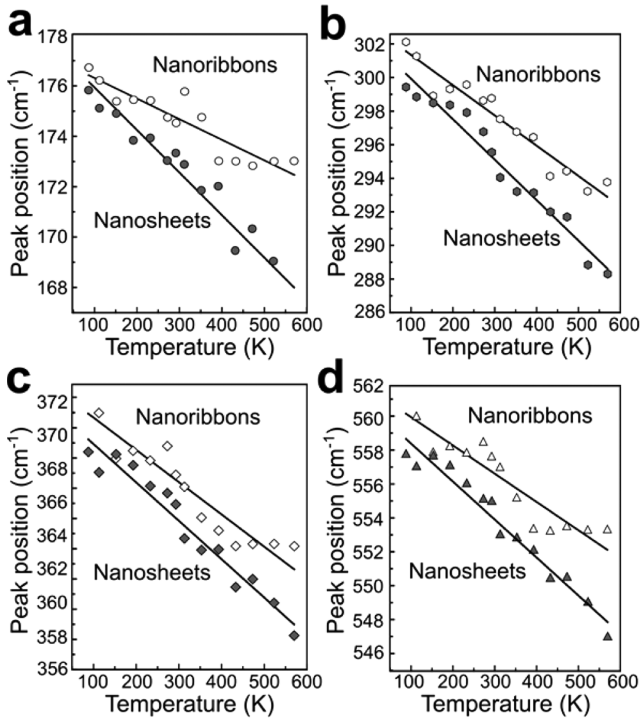

Figure 6. Temperature dependence of the four Raman peaks (a–d) measured for TiS_3 nanoribbon and nanosheet samples.

morphologies, nanoribbons and nanosheets, which were controlled during their synthesis. Both samples presented high crystallinity as evidenced by their X-ray diffraction, transmission electron microscopy, and electron diffraction characterization. The Raman spectra of the TiS_3 samples showed four prominent peaks corresponding to the excitation of A_g-type Raman modes, whose frequencies exhibit a linear temperature dependence over the entire temperature range studied from 88 to 570 K. This variation with temperature, similar to that observed in other 2D systems, is due to the anharmonic vibrations of the lattice (including contributions from the lattice thermal expansion). Interestingly, the temperature dependence of the Raman spectrum of TiS_3 nanosheets is noticeably stronger than that of TiS_3 nanoribbons, which we attribute to a lower interlayer coupling for nanosheets than for nanoribbons. Finally, we found that the temperature evolution of the Raman modes of TiS_3 is very strong (stronger than that observed in other 2D semiconductors), and thus, Raman spectroscopy can be exploited as a noninvasive local probe to measure the temperature in TiS_3-based nanodevices.

4. MATERIALS AND METHODS

Synthesis of TiS_3 Nanoribbons and Nanosheets. The synthesis of TiS_3 nanoribbons and nanosheets has been accomplished by a solid–gas reaction of Ti powder (Goodfellow, 99.5% purity) with sulfur gas provided by the heating of sulfur powder (Merck, 99.99% purity) into a vacuum-sealed ampule at 550 and 400 °C, respectively, during 15 days. The procedure is outlined in refs 31 and 32. TiS_3 powders have been structurally characterized by X-ray diffraction in a Panalytical X'pert Pro X-ray diffractometer (Cu Kα radiation (λ = 1.5406 Å)). All diffraction peaks can be attributed to the monoclinic phase of TiS_3 ($P2_1/m$ space group).

The as-prepared TiS_3 nanoribbon and nanosheet samples (composed of ribbons and flakes 100–300-nm thick) were simply transferred onto SiO_2/Si substrates to characterize their temperature-dependent Raman spectra.

Temperature-Dependent Raman Spectroscopy. For temperature-dependent Raman spectroscopy, we used a Renishaw inVia confocal Raman microscope with backscattering configuration. All experiments were carried out in ambient Ar at 5 mW laser power and 532 nm laser source with identical conditions. For carrying out the temperature-dependent Raman spectroscopy experiments, the Raman spectra were recorded by varying the temperature in the range of 88–

DOI: 10.1021/acsami.5b07492
ACS Appl. Mater. Interfaces 2015, 7, 24185–24190

Table 1. Summary of the First-Order Temperature Coefficients Reported for the Different Raman Modes of Several Two-Dimensional Materials

material	temperature coefficient (cm^{-1} K^{-1})				ref
graphene	χG		χ2D		
single layer graphene	−0.016		−0.026		28
single layer RGO	−0.029		∼0		
six-layer EG	−0.014		−0.01		
two-layer GNR	−0.030		∼0		
six-layer GNR	−0.018		−0.026		
TMDCs	χE^1_{2g}	χA_{1g}	2LA(M)	A_{1g}(M) + LA(M)	
single layer MoS_2	−0.013	−0.016			41
few-layer MoS_2	−0.016	−0.011			42
single layer WS_2	−0.006	−0.006	−0.008	−0.01	43
few-layer WS_2	−0.008	−0.004			43
	χA_{1g}	χA^2_{2u}			
single layer $MoSe_2$	−0.0054	−0.0086			45
few-layer $MoSe_2$	−0.0045	−0.0085			45
	χE^1_{2g}	χA_{1g}	A_{1g}+LA	2A_{1g}-LA	
single layer WSe_2	−0.0048	−0.0032	−0.0067	−0.0067	45
black phosphorus	χA_{1g}	χB_{2g}	χA_{2g}		
black phosphorus	−0.008	−0.013	−0.014		44
trichalcogenides			χ A_{1g} modes		
TiS_3 nanoribbons	−0.008	−0.018	−0.021	−0.016	this work
TiS_3 nanosheets	−0.022	−0.025	−0.024	−0.017	this work

570 K using low temperature measurements by liquid N_2 and a high temperature cell.

AUTHOR INFORMATION

Corresponding Authors

*E-mail: andres.castellanos@imdea.org.

*E-mail: datta099@gmail.com or dj.late@ncl.res.in.

Notes

The authors declare no competing financial interest.

ACKNOWLEDGMENTS

D.J.L. would like to thank Prof. C. N. R. Rao (FRS), JNCASR, and ICMS Bangalore (India) for encouragement and support. This work was supported by the Dutch Organization for Fundamental research (NWO/FOM). A.C-G. acknowledges financial support by BBVA Foundation through the fellowship "I Convocatoria de Ayudas Fundacion BBVA a Investigadores, Innovadores y Creadores Culturales" (project: "Semiconductores ultradelgados: hacia la optoelectronica flexible"). The Mire group acknowledges F. Moreno for technical support. The research work was supported by Department of Science and Technology (Government of India) under Ramanujan Fellowship to D.J.L. (Grant No. SR/S2/RJN-130/2012), NCL-MLP Project Grant 028626, DST-SERB Fast-Track Young Scientist Project Grant No. SB/FT/CS-116/2013, Broad of Research in Nuclear Sciences (BRNS) Grant No. 34/14/20/2015 (Government of India), and partial support by the INUP IITB project sponsored by DeitY, MCIT, Government of India, and CINT Proposal #U2015A0083 (USA).

REFERENCES

(1) Novoselov, K. S.; Geim, a K.; Morozov, S. V.; Jiang, D.; Zhang, Y.; Dubonos, S. V.; Grigorieva, I. V.; Firsov, A. A. Electric field effect in atomically thin carbon films. *Science* **2004**, *306* (5696), 666−669.

(2) Novoselov, K. S.; Jiang, D.; Schedin, F.; Booth, T. J.; Khotkevich, V. V.; Morozov, S. V.; Geim, a K. Two-dimensional atomic crystals. *Proc. Natl. Acad. Sci. U. S. A.* **2005**, *102* (30), 10451−10453.

(3) Coleman, J. N.; Lotya, M.; O'Neill, A.; Bergin, S. D.; King, P. J.; Khan, U.; Young, K.; Gaucher, A.; De, S.; Smith, R. J.; Shvets, I. V.; Arora, S. K.; Stanton, G.; Kim, H.-Y.; Lee, K.; Kim, G. T.; Duesberg, G. S.; Hallam, T.; Boland, J. J.; Wang, J. J.; Donegan, J. F.; Grunlan, J. C.; Moriarty, G.; Shmeliov, A.; Nicholls, R. J.; Perkins, J. M.; Grieveson, E. M.; Theuwissen, K.; McComb, D. W.; Nellist, P. D.; Nicolosi, V. Two-dimensional nanosheets produced by liquid exfoliation of layered materials. *Science* **2011**, *331* (6017), 568−571.

(4) Huang, X.; Zeng, Z.; Zhang, H. Metal dichalcogenide nanosheets: preparation, properties and applications. *Chem. Soc. Rev.* **2013**, *42* (5), 1934−1946.

(5) Wang, Q. H.; Kalantar-Zadeh, K.; Kis, A.; Coleman, J. N.; Strano, M. S. Electronics and optoelectronics of two-dimensional transition metal dichalcogenides. *Nat. Nanotechnol.* **2012**, *7* (11), 699−712.

(6) Lv, R.; Robinson, J. A.; Schaak, R. E.; Sun, D.; Sun, Y.; Mallouk, T. E.; Terrones, M. Transition Metal Dichalcogenides and Beyond: Synthesis, Properties, and Applications of Single- and Few-Layer Nanosheets. *Acc. Chem. Res.* **2015**, *48* (1), 56−64.

(7) Koppens, F. H. L.; Mueller, T.; Avouris, P.; Ferrari, A. C.; Vitiello, M. S.; Polini, M. Photodetectors based on graphene, other two-dimensional materials and hybrid systems. *Nat. Nanotechnol.* **2014**, *9* (10), 780−793.

(8) Xia, F.; Wang, H.; Xiao, D.; Dubey, M.; Ramasubramaniam, A. Two-dimensional material nanophotonics. *Nat. Photonics* **2014**, *8* (12), 899−907.

(9) Buscema, M.; Island, J. O.; Groenendijk, D. J.; Blanter, S. I.; Steele, G. A.; van der Zant, H. S. J.; Castellanos-Gomez, A. Photocurrent generation with two-dimensional van der Waals semiconductors. *Chem. Soc. Rev.* **2015**, *44* (11), 3691−3718.

(10) Choi, W.; Cho, M. Y.; Konar, A.; Lee, J. H.; Cha, G.-B.; Hong, S. C.; Kim, S.; Kim, J.; Jena, D.; Joo, J.; Kim, S. High-detectivity multilayer MoS(2) phototransistors with spectral response from ultraviolet to infrared. *Adv. Mater.* **2012**, *24* (43), 5832−5836.

(11) Yin, Z.; Li, H.; Li, H.; Jiang, L.; Shi, Y.; Sun, Y.; Lu, G.; Zhang, Q.; Chen, X.; Zhang, H. Single-layer MoS2 phototransistors. *ACS Nano* **2012**, *6* (1), 74−80.

(12) Lopez-Sanchez, O.; Lembke, D.; Kayci, M.; Radenovic, A.; Kis, A. Ultrasensitive photodetectors based on monolayer MoS2. *Nat. Nanotechnol.* **2013**, *8* (7), 497−501.

(13) Lee, H. S.; Min, S.-W.; Chang, Y.-G.; Park, M. K.; Nam, T.; Kim, H.; Kim, J. H.; Ryu, S.; Im, S. MoS_2 nanosheet phototransistors with

DOI: 10.1021/acsami.5b07492
ACS Appl. Mater. Interfaces 2015, 7, 24185−24190

thickness-modulated optical energy gap. *Nano Lett.* **2012**, *12* (7), 3695−3700.
(14) Zhang, Y.; Ye, J.; Matsuhashi, Y.; Iwasa, Y. Ambipolar MoS2 thin flake transistors. *Nano Lett.* **2012**, *12* (3), 1136−1140.
(15) Lee, G.-H.; Cui, X.; Kim, Y. D.; Arefe, G.; Zhang, X.; Lee, C.-H.; Ye, F.; Watanabe, K.; Taniguchi, T.; Kim, P.; Hone, J. Highly Stable, Dual-Gated MoS2 Transistors Encapsulated by Hexagonal Boron Nitride with Gate-Controllable Contact, Resistance, and Threshold Voltage. *ACS Nano* **2015**, *9* (7), 7019−7026.
(16) Das, S.; Chen, H.-Y.; Penumatcha, A. V.; Appenzeller, J. High performance multilayer MoS2 transistors with scandium contacts. *Nano Lett.* **2013**, *13* (1), 100−105.
(17) Wu, W.; De, D.; Chang, S.-C.; Wang, Y.; Peng, H.; Bao, J.; Pei, S.-S. High mobility and high on/off ratio field-effect transistors based on chemical vapor deposited single-crystal MoS2 grains. *Appl. Phys. Lett.* **2013**, *102* (14), 142106.
(18) Radisavljevic, B.; Whitwick, M. B.; Kis, A. Integrated circuits and logic operations based on single-layer MoS2. *ACS Nano* **2011**, *5* (12), 9934−9938.
(19) Radisavljevic, B.; Radenovic, A.; Brivio, J.; Giacometti, V.; Kis, A. Single-layer MoS2 transistors. *Nat. Nanotechnol.* **2011**, *6* (3), 147−150.
(20) Huo, N.; Yang, S.; Wei, Z.; Li, S.-S.; Xia, J.-B.; Li, J. Photoresponsive and gas sensing field-effect transistors based on multilayer WS_2 nanoflakes. *Sci. Rep.* **2014**, *4*, 5209.
(21) Shanmugam, M.; Durcan, C. A.; Yu, B. Layered semiconductor molybdenum disulfide nanomembrane based Schottky-barrier solar cells. *Nanoscale* **2012**, *4* (23), 7399−7405.
(22) Pospischil, A.; Furchi, M. M.; Mueller, T. Solar-energy conversion and light emission in an atomic monolayer p-n diode. *Nat. Nanotechnol.* **2014**, *9* (4), 257−261.
(23) Groenendijk, D. J.; Buscema, M.; Steele, G. A.; Michaelis de Vasconcellos, S.; Bratschitsch, R.; van der Zant, H. S. J.; Castellanos-Gomez, A. Photovoltaic and photothermoelectric effect in a double-gated WSe2 device. *Nano Lett.* **2014**, *14* (10), 5846−5852.
(24) Baugher, B. W. H.; Churchill, H. O. H.; Yang, Y.; Jarillo-Herrero, P. Optoelectronic devices based on electrically tunable p-n diodes in a monolayer dichalcogenide. *Nat. Nanotechnol.* **2014**, *9* (4), 262−267.
(25) Li, M.-Y.; Shi, Y.; Cheng, C.-C.; Lu, L.-S.; Lin, Y.-C.; Tang, H.-L.; Tsai, M.-L.; Chu, C.-W.; Wei, K.-H.; He, J.-H.; Chang, W.-H.; Suenaga, K.; Li, L.-J. Epitaxial growth of a monolayer WSe2-MoS2 lateral p−n junction with an atomically sharp interface. *Science* **2015**, *349* (6247), 524−528.
(26) Latte, D. J.; Rout, S. C.; Chakravarty, D.; Ratha, D. Emerging Energy Applications of Two-Dimensional Layered Materials. *Can. Chem. Trans.* **2015**, *3* (118−157), 118−157.
(27) Kashid, R. V.; Late, D. J.; Chou, S. S.; Huang, Y.-K.; De, M.; Joag, D. S.; More, M. A.; Dravid, V. P. Enhanced field-emission behavior of layered MoS_2 sheets. *Small* **2013**, *9* (16), 2730−2734.
(28) Pokrovskii, V.; Zybtsev, S.; Gorlova, I. Torsional Strain of TaS 3 Whiskers on the Charge-Density Wave Depinning. *Phys. Rev. Lett.* **2007**, *98* (20), 206404.
(29) Sinchenko, A. A.; Latyshev, Y. I.; Zybtsev, S. G.; Gorlova, I. G.; Monceau, P. Point-contact spectroscopy of the charge-density-wave gap along the chains in NbSe 3. *Phys. Rev. B: Condens. Matter Mater. Phys.* **1999**, *60* (7), 4624−4628.
(30) Gorlova, I. G.; Pokrovskii, V. Y.; Zybtsev, S. G.; Titov, A. N.; Timofeev, V. N. Features of the conductivity of the quasi-one-dimensional compound TiS3. *J. Exp. Theor. Phys.* **2010**, *111* (2), 298−303.
(31) Island, J. O.; Buscema, M.; Barawi, M.; Clamagirand, J. M.; Ares, J. R.; Sánchez, C.; Ferrer, I. J.; Steele, G. A.; van der Zant, H. S. J.; Castellanos-Gomez, A. Ultrahigh Photoresponse of Few-Layer TiS 3 Nanoribbon Transistors. *Adv. Opt. Mater.* **2014**, *2* (7), 641−645.
(32) Island, J. O.; Barawi, M.; Biele, R.; Almazán, A.; Clamagirand, J. M.; Ares, J. R.; Sánchez, C.; van der Zant, H. S. J.; Álvarez, J. V.; D'Agosta, R.; Ferrer, I. J.; Castellanos-Gomez, A. TiS3 transistors with tailored morphology and electrical properties. *Adv. Mater.* **2015**, *27* (16), 2595−2601.
(33) Ferrer, I. J.; Ares, J. R.; Clamagirand, J. M.; Barawi, M.; Sánchez, C. Optical properties of titanium trisulphide (TiS3) thin films. *Thin Solid Films* **2013**, *535*, 398−401.
(34) Ferrer, I. J.; Maciá, M. D.; Carcelén, V.; Ares, J. R.; Sánchez, C. On the Photoelectrochemical Properties of TiS3 Films. *Energy Procedia* **2012**, *22*, 48−52.
(35) Molina-Mendoza, A. J.; Barawi, M.; Biele, R.; Flores, E.; Ares, J. R.; Sánchez, C.; Rubio-Bollinger, G.; Agraït, N.; D'Agosta, R.; Ferrer, I. J.; Castellanos-Gomez, A. Electronic Bandgap and Exciton Binding Energy of Layered Semiconductor TiS 3. *Adv. Electron. Mater.* **2015**, *1* (9), 1500126.
(36) Dai, J.; Zeng, X. C. Titanium Trisulfide Monolayer: Theoretical Prediction of a New Direct-Gap Semiconductor with High and Anisotropic Carrier Mobility. *Angew. Chem.* **2015**, *127* (26), 7682−7686.
(37) Kim, S.; Konar, A.; Hwang, W.-S.; Lee, J. H.; Lee, J.; Yang, J.; Jung, C.; Kim, H.; Yoo, J.-B.; Choi, J.-Y.; Jin, Y. W.; Lee, S. Y.; Jena, D.; Choi, W.; Kim, K. High-mobility and low-power thin-film transistors based on multilayer MoS2 crystals. *Nat. Commun.* **2012**, *3*, 1011.
(38) Guilmeau, E.; Berthebaud, D.; Misse, P. R. N.; Hébert, S.; Lebedev, O. I.; Chateigner, D.; Martin, C.; Maignan, A. ZrSe 3 -Type Variant of TiS 3: Structure and Thermoelectric Properties. *Chem. Mater.* **2014**, *26* (19), 5585−5591.
(39) Gard, P.; Cruege, F.; Sourisseau, C.; Gorochov, O. Single-crystal micro-Raman studies of ZrS3, TiS3 and several Zr1-xTixS3 compounds ($0 < x \leqslant 0.33$). *J. Raman Spectrosc.* **1986**, *17* (3), 283−288.
(40) Late, D. J.; Maitra, U.; Panchakarla, L. S.; Waghmare, U. V.; Rao, C. N. R. Temperature effects on the Raman spectra of graphenes: dependence on the number of layers and doping. *J. Phys.: Condens. Matter* **2011**, *23* (5), 055303.
(41) Lanzillo, N. A.; Glen Birdwell, A.; Amani, M.; Crowne, F. J.; Shah, P. B.; Najmaei, S.; Liu, Z.; Ajayan, P. M.; Lou, J.; Dubey, M.; Nayak, S. K.; O'Regan, T. P. Temperature-dependent phonon shifts in monolayer MoS2. *Appl. Phys. Lett.* **2013**, *103* (9), 093102.
(42) Thripuranthaka, M.; Kashid, R. V.; Sekhar Rout, C.; Late, D. J. Temperature dependent Raman spectroscopy of chemically derived few layer MoS2 and WS2 nanosheets. *Appl. Phys. Lett.* **2014**, *104* (8), 081911.
(43) M, T.; Late, D. J. Temperature dependent phonon shifts in single-layer WS(2). *ACS Appl. Mater. Interfaces* **2014**, *6* (2), 1158−1163.
(44) Late, D. J. Temperature dependent phonon shifts in few-layer black phosphorus. *ACS Appl. Mater. Interfaces* **2015**, *7* (10), 5857−5862.
(45) Late, D. J.; Shirodkar, S. N.; Waghmare, U. V.; Dravid, V. P.; Rao, C. N. R. Thermal expansion, anharmonicity and temperature-dependent Raman spectra of single- and few-layer $MoSe_2$ and WSe_2. *ChemPhysChem* **2014**, *15* (8), 1592−1598.
(46) Calizo, I.; Balandin, A. A.; Bao, W.; Miao, F.; Lau, C. N. Temperature dependence of the Raman spectra of graphene and graphene multilayers. *Nano Lett.* **2007**, *7* (9), 2645−2649.

DOI: 10.1021/acsami.5b07492
ACS Appl. Mater. Interfaces 2015, 7, 24185−24190